

Scientific paper

# A Highly Accurate, Analytic Potential Energy Surface of the Hydrogendifluoride Anion in the Gas Phase

Jernej Stare

National Institute of Chemistry, Hajdrihova 19, SI-1000 Ljubljana, Slovenia

\* Corresponding author: E-mail: jernej.stare@ki.si

Received: 06-05-2011

Dedicated to Professor Dušan Hadži on the occasion of his 90<sup>th</sup> birthday

## Abstract

We calculated the full three-dimensional potential energy surface (PES) of an isolated hydrogendifluoride anion (FHF<sup>-</sup>) in the electronic ground state at a very accurate Coupled Cluster approach and large correlation-consistent valence triple-zeta basis set [CCSD(T)/aug-cc-pVTZ]. The PES was evaluated at more than 30.000 points corresponding to different geometries of the system. Analytical form of the PES was expressed in an internal coordinate set which included the F...F separation (internal coordinate  $R$ ) and the longitudinal and transversal projection (internal coordinates  $x$  and  $y$ ) of the proton position on the F...F line. For each constant value of  $x$  a two-dimensional fit along  $y$  and  $R$  was performed by using displaced Gaussian functions. The fitted parameters of Gaussians were then spline-interpolated along  $x$  to get the final analytical form of the three-dimensional PES. The maximum fitting error was less than 0.01 kcal/mol in the lowest 20 kcal/mol region of the PES, yielding an accurate and conveniently formulated surface which can be readily used for advanced calculations, including fully coupled anharmonic vibrational analysis and quantum dynamics simulation.

**Keywords:** Hydrogendifluoride anion, short hydrogen bonding, potential energy surface, vibrational dynamics, coupled cluster calculations, three-dimensional fitting

## 1. Introduction

Hydrogen bonding is an important interaction which governs the structure and properties of a variety of molecular systems, including highly relevant biological molecules such as enzymes, or materials with industrial application. Despite the enormous amount of experimental and computational work devoted to hydrogen bond research, this phenomenon remains poorly understood in many crucial aspects. Particularly this holds for examples of extremely short hydrogen bonds with notably pronounced geometric and spectroscopic features, such as a broad and red-shifted hydrogen stretching band in the vibrational spectra and <sup>1</sup>H NMR resonance signal of the proton at very low fields, etc. Since Kreevoy and Cleland postulated the role of the so called »low barrier hydrogen bonding« in the enzyme catalysis,<sup>1</sup> theoretical and experimental research of such hydrogen bonds (also dubbed »short and strong hydrogen bond«) has gained momentum and the improved understanding of many properties of short hydrogen bonding has remained to date a challenge and subject of various studies.

Perhaps the most essential and universal feature required for the understanding of any observable quantity of a chemical system, including short hydrogen bonding, is the potential energy surface (PES), which governs virtually all the aspects of structure and dynamics of the system. Not surprisingly, the features of the PES have been for long at the focal point of theoretical and experimental hydrogen bond research.<sup>2–8</sup> However, adequate sampling of the PES has proved to be a very demanding task for various reasons. First, the PES is an extremely complex function. For a system of  $N$  atoms, the dimensionality of the PES is  $3N-6$ , which renders the computational evaluation of the complete PES virtually impossible for all but smallest systems. Second, very accurate and demanding computational approach is often needed in order to faithfully reproduce the PES and its important features, such as curvatures (vibrational frequencies) or barrier heights. This holds particularly for short hydrogen bonds; for instance, accurate evaluation of proton transfer barrier of malonaldehyde requires the use of Coupled Cluster approach, while the popular, widely used and cost-efficient DFT methodologies severely underestimate the barrier.<sup>9,10</sup>

The hydrogen difluoride anion ( $\text{FHF}^-$ ) in the gas phase is arguably the simplest example of an extremely short and strong hydrogen bond. The equilibrium F...F separation determined from rotational constants by diode laser spectroscopy is  $2.7777 \text{ \AA}^{11}$  and the bond energy is estimated to  $45.8 \text{ kcal/mol}^{12}$  which probably qualifies it as the shortest and strongest hydrogen bond ever known. Given the simplicity of the system whose structure is fully determined by only three internal nuclear degrees of freedom,  $\text{FHF}^-$  represents a popular benchmark example which has been extensively elaborated in the past by advanced computational techniques, including the evaluation of the full 3D PES or its selected 2D subspace over a wide range of coordinate values.<sup>13–16</sup> Indeed, on the basis of accurate calculations of anharmonic vibrational levels via the solving of the three-dimensional vibrational Schrödinger equation the initial experimental assignment of the asymmetric F...H...F stretching band, recorded by infrared diode laser spectroscopy,<sup>11,17</sup> was changed from  $1849$  to  $1331 \text{ cm}^{-1}$ .<sup>18</sup> Our experience includes an anharmonic vibrational calculation in the reduced 2D coordinate space of the symmetric and asymmetric F...H...F stretching modes assuming linearity and neglecting the bending degree of freedom.<sup>19</sup> A similar 2D study has been performed by Elghobashi et al., also yielding excellent agreement of the symmetric stretching frequency with the experimental value, but much less so for the asymmetric stretching, probably due to the neglected coupling to the bending degree of freedom.<sup>20</sup> A very recent example of research which benefits from the hydrogendifluoride system is at the level of particle physics, examining the nature of the hydrogen bond-like interaction in the analog complex, where the proton is substituted by a muon ( $\text{F}\dots\mu\dots\text{F}$ ).<sup>21</sup>

Despite its simplicity, the calculated properties of  $\text{FHF}^-$  via the PES have been proved to exhibit very large variations with the applied level of theory – much larger than with most of other benchmark systems,<sup>16,22,23</sup> leaving open door for further improvement in the evaluation of the PES by employing state-of-the-art accurate methodologies, feasible to run in massive quantities on modern computers. Also, while the PES of  $\text{FHF}^-$  has been evaluated for a number of times in the past, there is still a lack of experience in designing a strategy for the construction of a reliable PES in an analytic form. Thus, the attributes of the pointwise evaluation of the PES, including the sampling density and coordinate range, together with the fitting strategy still remain a largely open issue. The scope of this article is to provide an accurate 3D PES of isolated  $\text{FHF}^-$  by means of a highly accurate *ab initio* methodology, together with a concise sampling and fitting strategy, ultimately yielding a convenient, analytic form of the PES. This form, available on request as a Fortran code, may be used for any advanced study which relies on a fast and accurate evaluation of the PES at a large number of points. Examples of such calculations are the solving of a fully coupled 3D vibrational Schrödinger equation or a

quantum dynamics simulation of the system. Given that  $\text{FHF}^-$  is a popular benchmark example essential for the understanding of short hydrogen bonding, such applications are expected to remain challenging in the future, despite that they may have been to some extent already elaborated in the past.

## 2. Computational

*Level of theory.* The PES of  $\text{FHF}^-$  was evaluated by pointwise calculations according to the strategy presented below. All calculations were carried out by the *Gaussian 03* program package.<sup>24</sup> The highly reliable and accurate Coupled Cluster methodology CCSD(T) was chosen as model chemistry. The basis set was taken from the Dunning correlation-consistent line of split-valence basis sets differing in the number of levels representing the valence orbitals (from 2 to 6), to which diffuse functions were added. A straightforward test of the basis set performance are the optimized F...F separation and harmonic frequencies, listed in Table 1.

**Table 1.** Optimized F...F separation and harmonic frequencies of the isolated  $\text{FHF}^-$  ion ( $\nu_1$  – symmetric F...H...F stretching;  $\nu_2$  – F...H...F bending;  $\nu_3$  – asymmetric F...H...F stretching), calculated by the CCSD(T) approach and various basis sets. *Nb* denotes the number of basis functions.

basis set	$R_{FF}$ [Å]	$\nu_1$ [cm <sup>-1</sup> ]	$\nu_2$ [cm <sup>-1</sup> ]	$\nu_3$ [cm <sup>-1</sup> ]	<i>Nb</i>
aug-cc-pVDZ	2.3037	613	1330	1054	55
aug-cc-pVTZ	2.2802	641	1366	1272	115
aug-cc-pVQZ	2.2788	639	1348	1199	206
aug-cc-pV5Z	2.2789	639	1335	1172	334
aug-cc-pV5Z (on F)*	2.2780	639	1334	1175	381
aug-cc-pV6Z (on H)	2.2777	583	1286	1331	–
experimental	2.2777	583	1286	1331	–

\* The aug-cc-pV6Z basis set is not available for fluorine atom.

It can be seen that the frequency of the asymmetric F...H...F stretching mode ( $\nu_3$ ) exhibits high sensitivity to the basis set size. While the criterion for satisfactory convergence is somewhat arbitrary, we feel that the aug-cc-pVQZ basis set represents a sound compromise between accuracy and computational cost and may be quite safely assumed to yield convergent properties of the system. However, due to the fact that the appropriate sampling of the 3D PES requires thousands of energy evaluations, and as computational time increases by about an order of magnitude when the basis set size is doubled, we restricted ourselves in the present work to the smaller aug-cc-pVTZ basis set, which allows the PES calculation to be done in a reasonable time. We believe that the difference between triple- and quadruple-zeta basis set are not notably reflected

ted in main features of the PES, and the choice of the smaller basis set is still legitimate for devising the fitting strategy. Also it should be noted that any comparison of the tabulated geometry and vibrational frequencies with the experimental values is of very limited value, since these calculations do not take into account anharmonicity and nuclear quantum effects which are crucial for both vibrational properties and geometry of the system.

**Internal coordinate system.** The internal coordinate system in which the PES was represented, was constructed in the following way. The origin of the internal coordinate system was set to the midpoint between the fluorine nuclei. The  $x$  axis of the coordinate system was placed along the line that connects the fluorines and the  $y$  axis was set to be perpendicular to  $x$  (Fig. 1). Thus, the longitudinal and transversal projection of the proton position on the F...F line represent the  $x$  and  $y$  coordinate, respectively; the third coordinate is the F...F separation ( $R_{FF}$ ).

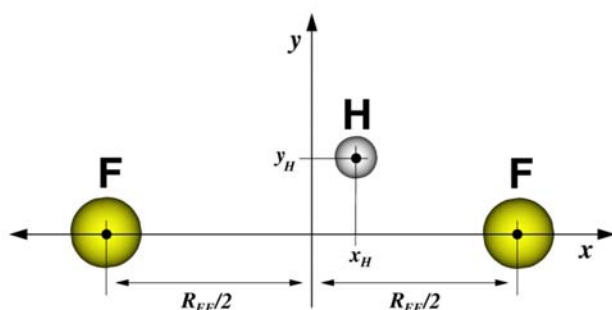


Figure 1. Definition of the three internal coordinates  $x$ ,  $y$  and  $R_{FF}$ .

Furthermore, it is convenient to represent the F...F separation as an offset from the equilibrium separation ( $R$ ) rather than with the absolute value ( $R_{FF}$ ):  $R = R_{FF} - R_{FF}^0$ , where  $R_{FF}^0$  is the equilibrium F...F distance of 2.2802 Å. Thus, the structure with all the three internal coordinates equal to zero represents the global minimum geometry. Evidently, the potential expressed in this coordinate system features the following symmetry:

$$V(x,y,R) = V(-x,y,R) = V(x,-y,R) = V(-x,-y,R). \quad (1)$$

It should also be noted that the reduced masses within this coordinate system are constant (coordinate-independent) and kinetically orthogonal.

**Construction of the PES.** The 3D PES was constructed as a set of 2D “slices” in the following way. For each distinct value of  $R$ , a 2D ( $x,y$ ) surface was pointwise evaluated by moving the proton on a uniform grid with the restriction that its separation from either fluorine atom was at least 0.75 Å. The grid resolution was 0.05 Å, which ensured smooth fits without unwanted artifacts (see below). This resulted in about 700–1500 points per 2D surface. The construction of a 2D surface for  $R = 0$  is presented in Fig. 2.

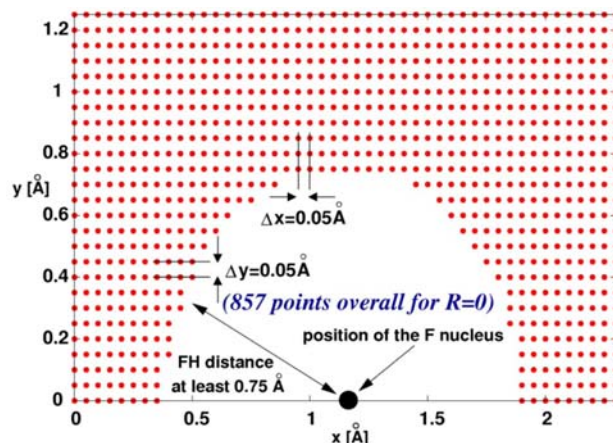


Figure 2. Positions of hydrogen atom (red dots) in the construction of a 2D slice of the PES at a constant F...F distance.

For each 2D slice the ranges of the coordinates  $x$  and  $y$  were chosen such that the potential energy at the boundaries was at least 40 kcal/mol above the minimum, and the symmetry of the potential was exploited. The 2D slices presented above were calculated for a series of different F...F separations between 1.7802 and 4.7802 Å and the step in F...F was 0.05 Å, resulting in 61 two-dimensional slices. The internal coordinate ranges were the following:  $x \in [0.00, 2.70 \text{ Å}]$ ,  $y \in [0.00, 2.00 \text{ Å}]$ ,  $R \in [-0.50, 2.50 \text{ Å}]$ . The complete PES evaluation totaled in about 30,000 single point calculations at the CCSD(T)/aug-cc-pVTZ level of theory. The strategy of pointwise calculations was assisted by preliminary evaluations of the PES at a much less CPU-intensive B3LYP/6-31+G(d,p) level.

**Fitting.** Technically the most straightforward fitting procedure should include a three-dimensional parametrized function  $f(x,y,R;A)$  where  $A$  is an array of parameters that should be chosen in such a way to minimize the penalty function  $P$ :

$$P(A) \equiv \sum_i w_i [f(x_i, y_i, R_i; A) - V(x_i, y_i, z_i; A)]^2 \quad (2)$$

where the summation is performed over all the points ( $x_i, y_i, R_i$ ) for which the values of  $V$  have been determined by quantum chemical calculations. It is also reasonable to use a weighting scheme that stresses the importance of points with low energy; the values of weights ( $w_i$ ) can be, for example, inversely proportional to  $V(x_i, y_i, R_i)$ . In our calculations the weights have been determined by the expression  $w_i = 1/[V(x_i, y_i, R_i) + K]$ , with a small constant  $K$  of 0.01 – 0.1 kcal/mol being used to avoid singularities in  $w_i$ .

The main difficulty of a supposed 3D fit outlined above lies in the fact that the required set of parameters for a 3D function is very large; based on our experience from 2D fitting of Gaussian-type functions which typi-

cally included about 60 parameters,<sup>19,25,26</sup> a reasonable 3D analog would involve at least 500 parameters. Additionally, the dataset is very large – in the present case the full 3D dataset includes about 30.000 points, while typical 2D datasets have at most a few hundreds of points. Also the number of iterations required for the minimization of  $P$  in a 3D fit is supposed to be much larger than for 2D fits; thus computational time for a 3D fit would be at least three to four orders of magnitude larger than for a 2D fit, which can usually be managed on the scale of ten minutes. Apart from these drawbacks, 3D fits are much more difficult to be controlled because of the inability of full visualization. Accordingly, we built our fitting strategy on 2D projections (“slices”) through the 3D PES in the following way:

- (1) Choose a 2D slice through the PES, with one coordinate being constant and the other two variables.
- (2) Perform a 2D fit along the variable coordinates based on the subset of the original dataset with the fixed coordinate having a constant value.
- (3) Repeat (2) for all possible slices characterized by the value of the fixed coordinate.
- (4) Link (interpolate) the 2D fitted parameters along the coordinate that remained fixed in the 2D fits.
- (5) Visualize the fitted function, and check it for smoothness and unwanted artifacts.

In the present work, three distinct interpolation schemes were used to obtain the analytic expression of the

full PES from the pointwise calculated dataset: (i) analytic expressions for two-dimensional slices through the PES were acquired by fitting of Gaussian-type functions (one linear and four non-linear fitted parameters per each Gaussian) to the corresponding subsets of points of the dataset; the fitting was based on a quasi-Newton minimization of a weighted penalty function<sup>27</sup> and, optionally, employed a large number of minimization cycles (about one million per fit) and very tight convergence criteria; (ii) the fitted parameters of two-dimensional slices were linked together along the third dimension by the cubic spline interpolation scheme; (iii) when necessary, additional points were added to the original dataset by means of the three-dimensional weighted Shepard interpolation utility of Renka.<sup>28,29</sup>

### 3. Results and Discussion

*Optimal fitting strategy.* The fact that the PES has been evaluated by successive 2D projections with variable  $x$  and  $y$  and at constant  $R$  suggests that the fitting should proceed equivalently, namely that the subsequent 2D Gaussian fits would be performed over  $x$  and  $y$  at constant  $R$  (an “ $xy$  slice”), and then the fitted parameters would be spline-interpolated along  $R$ . However, the other two options employing a swapped role of coordinates are in principle equally legitimate and merit consideration for fitting strategy. Fig. 3 displays the characteristic 2D slices

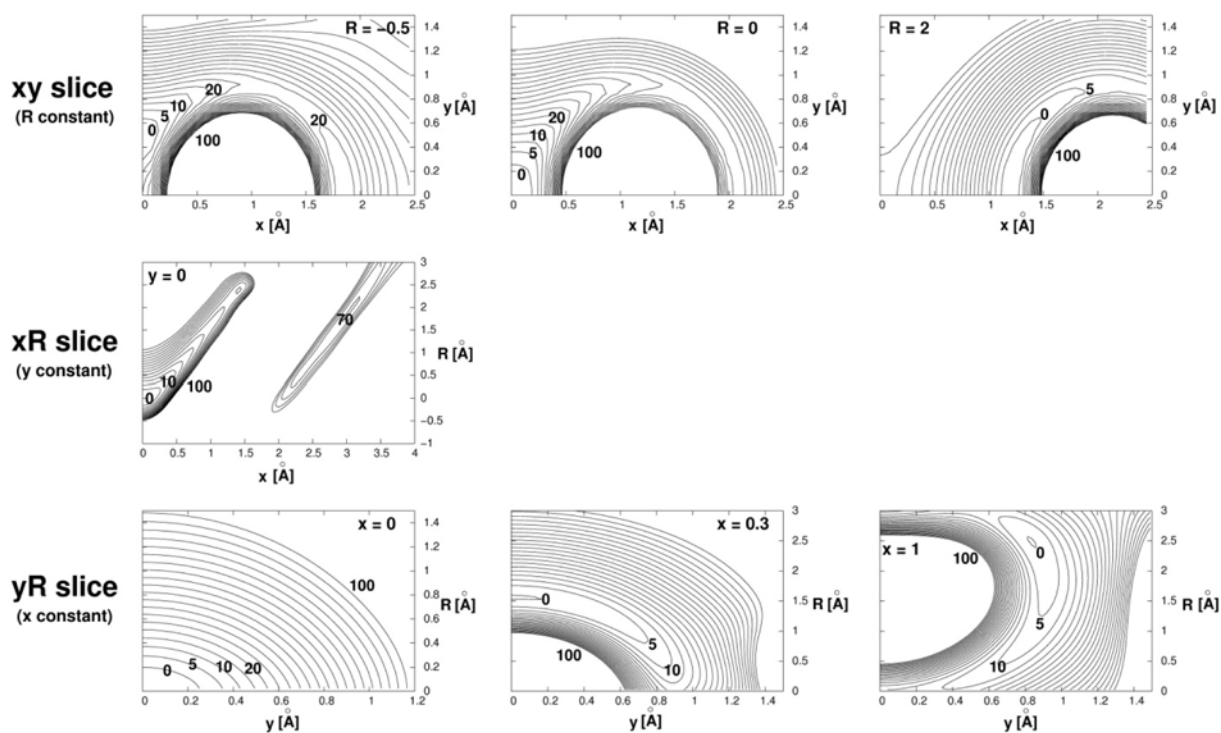


**Figure 3.** Contour plots of different 2D slices through the 3D PES of FHF<sup>-</sup>. Selected contours are labeled with the corresponding relative energies in kcal/mol and the corresponding values of the third (constant) coordinate (in Å) are listed.

through the 3D PES of  $\text{FHF}^-$ . Note that in each row one of the coordinates is held constant while the other two are variables.

The  $(x,y)$  slice (top line) evidently represents the most conventional representation of a 2D subset of the PES. The large high-energy circular area clearly corresponds to the hard-core potential experienced by the proton when being placed in the vicinity of the fluorine atom. Although visual appearance suggests that such slices can be smoothly connected by spline interpolation of the fitted parameters of the individual slices, we met severe difficulties in our attempts to smoothly pass between two successive slices along  $R$ . It is perhaps a bit surprising that the  $(y,R)$  slices (bottom line) delivered notably smoother interpolation of the fitted parameters along  $x$ . Additionally, the  $(y,R)$  slices were found to provide easier 2D fits and require less parameters than the  $(x,y)$  slices – the latter required 20 Gaussian functions for a good fit while the former required only 13. On the contrary, the  $(x,R)$  slices are considerably more sophisticated in shape and evidently more demanding for analytical fitting; as such they are not appropriate for the fitting strategy outlined in the Computational section. Therefore we proceeded with the fitting based on 2D projections of the PES as functions of  $y$  and  $R$  while  $x$  was constant at each distinct projection.

**Resolution of the dataset and fitting quality.** The fitting proceeded over 2D slices of the PES in which  $y$  and  $R$  were variables and  $x$  was held constant. Starting from the slice at  $x = 0.00 \text{ \AA}$ , a set of 13 displaced Gaussian functions of  $y$  and  $R$  was fitted to the dataset. After the fitting, we proceeded to the next slice (at  $x = 0.05 \text{ \AA}$ ) and repeated the fitting, using the fitted parameters from the previous surface as the initial guess. We subsequently repeated this procedure until the last 2D surface at  $x = 2.70 \text{ \AA}$ . The obtained series of fitted parameters of the 2D Gaussians, corresponding to surfaces at different values of  $x$ , were then spline-interpolated along  $x$  to yield the final form of the complete 3D PES. This function was subjected to fur-

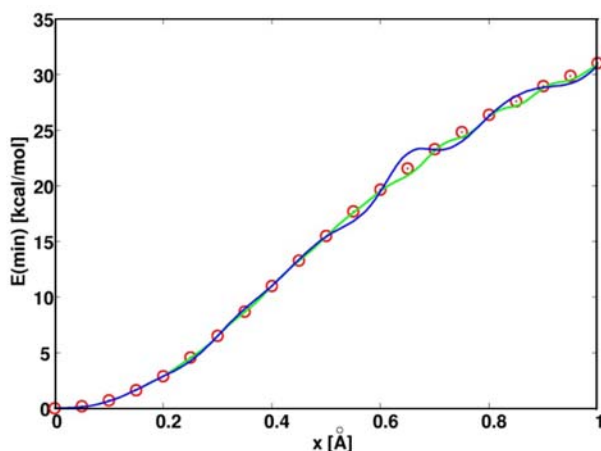


**Figure 4.** Minimum of the projection of the PES at constant  $x$  as a function of  $x$ . Blue line: resolution =  $0.050 \text{ \AA}$ ; green line: resolution =  $0.025 \text{ \AA}$ ; red circles: exact CCSD(T) values

her analysis. The analytical form of the 3D PES allows for making analytical minimum-energy projections along the desired coordinate. A minimum-energy profile along  $x$  is displayed in Fig. 4.

The blue line represents the minimum-energy profile of the PES by using exclusively the original data points. It should be stressed that subsequent 2D slices differ in  $x$  by  $0.05 \text{ \AA}$ . Clearly, while the energy curve is smooth and features no notable artifacts at small values of  $x$ , the shape becomes much less reasonable at  $x > 0.20 \text{ \AA}$ ; at  $x > 0.50 \text{ \AA}$  large discrepancies (several kcal/mol) between the fitted function and the original data (red circles) are observed. This indicates that the density of the original 2D slices along  $x$  is too low. Namely, when passing from one 2D surface to another, the fitting alters the parameters of the Gaussians; the difference between the “old” and “new” parameters is larger when the resolution in  $x$  is low and when subsequent surfaces are less similar to one another. Consequently, the interpolation of the parameters becomes harder and can lead to unwanted artifacts. The similarity of parameters between the consecutive fits (and thus the reliability of spline interpolation) can be enforced by limiting the number of cycles in the numerical fitting procedure, but this ultimately leads to poorer 2D fits and poor overall fit. The only way to overcome this problem is the increased resolution of the dataset, i.e. a more dense set of consecutive 2D surfaces. Since additional quantum calculations are not practical, we enlarged the original dataset by the three-dimensional interpolation utility of Renka.<sup>29</sup> This does not improve the quality of information contained in the original, pointwise calculated dataset, but helps the subsequent 2D fits to proceed more smoothly, because the surfaces become more similar to one another. The green line represents the minimum-energy projection of the PES, acquired at the double resolution in  $x$  ( $0.025 \text{ \AA}$ ), and the improvement is evident. Nevertheless, issues inherent to such fitting persist and further increase of the dataset is required to deliver a high precision 3D fit. Ultimately, when the original dataset of *ab initio* points is densified in the  $x$  direction by an order of magnitude (the resolution of the subsequent 2D surfaces is  $0.005 \text{ \AA}$  in  $x$ ), the fitting procedure described above yields an extremely accurate and smooth fit; the shape of the function is apparently flawless, and the root-mean-square fitting error in the lowest 20 kcal/mol region of the PES is only about  $0.002 \text{ kcal/mol}$ . The maximum offset of the fitted function from the original dataset is about  $0.01 \text{ kcal/mol}$ , which we believe is sufficient for quantitative spectroscopic application. The fitting error profile over the original data points in the lowest energy region is displayed in Fig. 5.

**Features of the PES.** Some major characteristics of the PES can be demonstrated by means of minimum-energy profiles along the selected internal coordinates, displayed in Fig. 6. The profile along  $R$  is displayed on top of Fig 6. For all but smallest F...F distances, the structure of the system is linear. Soon after the minimum ( $R > 0.10 \text{ \AA}$ )

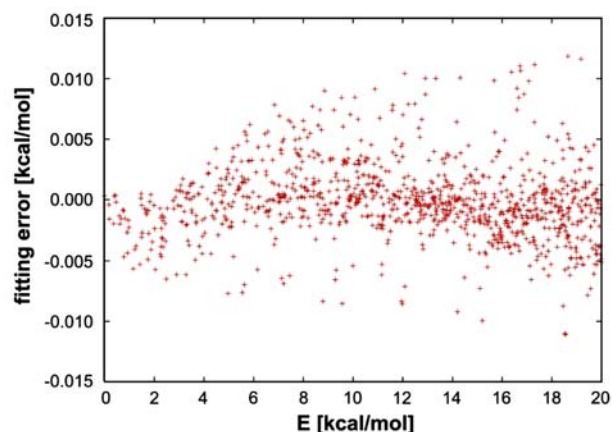


**Figure 5.** Fitting error as function of the relative energy in the lowest 20 kcal/mol region of the PES. Each point represents the energy difference between the fitted function and the corresponding dataset value.

the structure becomes asymmetric with the proton located nearer to one fluorine nucleus. At large values of  $R$  the energy approaches the dissociation limit calculated to 44.5 kcal/mol, which is in excellent agreement with experimental findings.<sup>12</sup> The curve features a profile of Morse-like function characteristic of many covalent bonds, indicating the strongly covalent nature of hydrogen bonding in  $\text{FHF}^-$ . In contrast to  $R$  the bending energy profile along  $y$  (Fig. 6, middle) is slightly steeper and far above dissociation in the displayed region. The latter is due to the fact that when constraining the internal (bending) coordinate  $y$  to relatively high values, the negatively charged fluorine atoms become exposed to one another in a strongly repulsive interaction. However, due to the fact that the sampled  $\text{F}\cdots\text{F}$  separation was limited to less than 5 Å, the fluorines cannot accordingly relax to larger separation, which leads to overestimated values of the potential above  $y = 0.7$  Å. Nevertheless, this effect is substantial only at the regions of the PES which are more than 40 kcal/mol above the minimum, so this artifact is practically irrelevant for lower vibrational states. Finally, the minimum-energy profile along the  $x$  (stretching) coordinate is displayed in the bottom of Fig. 6, featuring a sigmoidal shape. Again, the structure is linear until the bending component outbalances the dissociation tendency on the increasing displacement of the proton from the midpoint of the  $\text{F}\cdots\text{F}$  line. The small bump at  $x \approx 1.4$  Å originates from the fixation of  $R$  to 2.5 Å, which is the maximum  $\text{F}\cdots\text{F}$  separation sampled in this work. Similarly as with the potential along  $y$ , this ultimately leads to the artifact that at very large values of  $x$  the energy is above the dissociation limit.

As can be seen from the features displayed above, the fitted PES is of very high quality in the region of lower vibrational states. The fact that the coordinate ranges were rather limited slightly impairs the quality of the PES for the highly excited vibrational levels and renders any dynamical

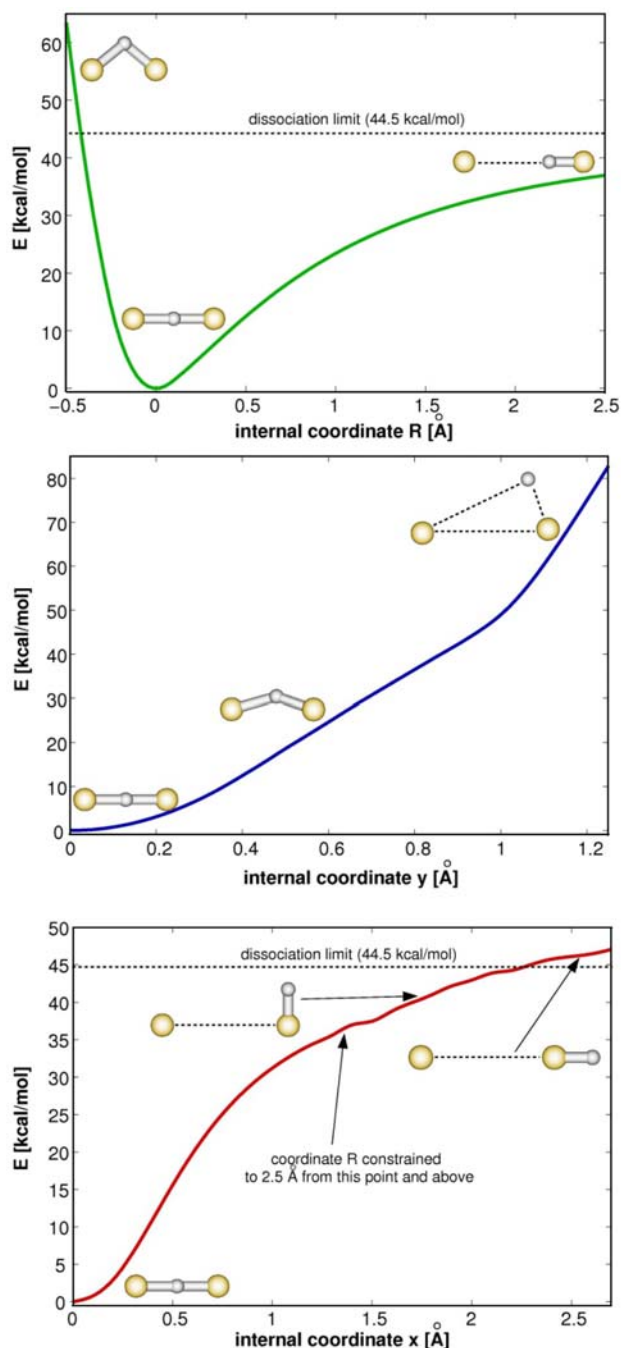


**Figure 6.** Minimum-energy curve of the PES along the three internal coordinates with selected characteristic structures.

processes associated with the dissociation process less reliable. While the calculated dissociation energy is in excellent agreement with the experimental data, the PES is clearly inadequately sampled in the region which corresponds to dissociation. A reliable inclusion of the dissociative part of the PES would require much additional effort which is beyond the scope of this work.

At the bottom line it should be noted that the ultimate verification of the presented calculations are actual ob-

servables, such as anharmonic vibrational frequencies, which can be derived from the PES and compared to the experimental data. This part, together with a concise comparison with previous computational experience, remains a challenge for the near future.

## 4. Conclusions

The three-dimensional potential energy surface of the isolated hydrogendifluoride anion in the electronic ground state has been calculated at over 30.000 distinct geometries using the highly accurate CCSD(T)/aug-cc-pVTZ computational approach. A concise internal coordinate set has been chosen, allowing for expressing the PES in a convenient analytical representation, and an optimal fitting strategy was devised, ultimately leading to a very accurate and reliable analytic form of the PES in the region of up to 40 kcal/mol above the minimum. With the fitting error being of an order of only a few thousandths of kcal/mol in the low energy region, the PES is suitable for computational treatment of the vibrational dynamics at quantitative precision, as long as highly excited vibrational levels are not significant. As all major characteristic features of the PES are virtually independent of the actual level of theory, at least when accurate methodologies and large basis sets are used, the present fitting approach is trivially applicable to improved PES calculations which may be feasible in the future.

## 5. Acknowledgements

I owe deep and sincere gratitude to Professor Dušan Hadži, who introduced me to hydrogen bond research and supervised my work as a mentor and teacher for the entire course of my scientific career. His ever lasting curiosity, passion and commitment for science combined with his permanent readiness to consult and help, and his warm personal approach often spiced by a good dose of humour keeps inspiring his coworkers and helps us greatly in our professional and personal development. This work benefited from the Slovenian Research Agency program group (P1-0012) and project (J1-2014) funding.

## 6. References

1. W. W. Cleland, M. M. Kreevoy, *Science* **1994**, *264*, 1887–1890.
2. T. Carrington, W. H. Miller, *J. Chem. Phys.* **1986**, *84*, 4364–4370.
3. D. H. Zhang, Q. Wu, J. Z. H. Zhang, M. Von Dirke, Z. Bačić, *J. Chem. Phys.* **1995**, *102*, 2315–2325.
4. F. Sebastianelli, Y. S. Elmatad, H. Jiang, Z. Bačić, *J. Chem. Phys.* **2006**, *125*, 164313.
5. Z. Dega-Szafran, M. Grundwald-Wyspiańska, M. Szafran, *J. Mol. Struct.* **1992**, *275*, 159–165.
6. J. Mavri, J. Grdadolnik, *J. Phys. Chem. A* **2001**, *105*, 2039–2044.
7. I. Matanović, N. Došlić, *J. Phys. Chem. A* **2005**, *109*, 4185–4194.
8. M. Petković, J. Novak, N. Došlić, *Chem. Phys. Lett.* **2009**, *474*, 248–252.
9. C. S. Tautermann, A. F. Voegelé, T. Loerting, K. R. Liedl, *J. Chem. Phys.* **2002**, *117*, 1962–1966.
10. G. V. Mil'nikov, K. Yagi, T. Taketsugu, H. Nakamura, K. Hirao, *J. Chem. Phys.* **2003**, *119*, 10–13.
11. K. Kawaguchi, E. Hirota, *J. Chem. Phys.* **1986**, *84*, 2953–2960.
12. P. G. Wenthold, R. S. Squires, *J. Phys. Chem.* **1995**, *99*, 2002–2005.
13. J. Almlöf, *Chem. Phys. Lett.* **1972**, *17*, 49–52.
14. V. Špirko, A. Čejchan, G. H. F. Diercksen, *Chem. Phys.* **1991**, *151*, 45–58.
15. K. Yamashita, K. Morokuma, C. Leforestier, *J. Chem. Phys.* **1993**, *99*, 8848–8855.
16. C. L. Janssen, W. D. Allen, H. F. Schaefer III, J. M. Bowman, *Chem. Phys. Lett.* **1986**, *131*, 352–358.
17. K. Kawaguchi, E. Hirota, *J. Mol. Struct.* **1995**, *352/353*, 389–394.
18. K. Kawaguchi, E. Hirota, *J. Chem. Phys.* **1987**, *87*, 6838–6841.
19. J. Stare, G. G. Balint-Kurti, *J. Phys. Chem. A* **2003**, *107*, 7204–7214.
20. N. Elghobashi, L. González, *J. Chem. Phys.* **2006**, *124*, 174308.
21. R. Blinc, G. Lahajnar, A. Potočnik, *Acta Chim. Slov.* **2011**, *in press*.
22. Z. Latajka, Y. Bouteiller, S. Scheiner, *Chem. Phys. Lett.* **1995**, *234*, 159–164.
23. S. Kawahara, T. Uchimaru, K. Taira, *Chem. Phys.* **2001**, *273*, 207–216.
24. M. J. Frisch, G. W. Trucks, H. B. Schlegel, G. E. Scuseria, M. A. Robb, J. R. Cheeseman, J. A. Montgomery Jr., T. Vreven, K. N. Kudin, J. C. Burant, J. M. Millam, S. S. Iyengar, J. Tomasi, V. Barone, B. Mennucci, M. Cossi, G. Scalmani, N. Rega, G. A. Petersson, H. Nakatsuji, M. Hada, M. Ehara, K. Toyota, R. Fukuda, J. Hasegawa, M. Ishida, T. Nakajima, Y. Honda, O. Kitao, H. Nakai, M. Klene, X. Li, J. E. Knox, H. P. Hratchian, J. B. Cross, C. Adamo, J. Jaramillo, R. Gomperts, R. E. Stratmann, O. Yazyev, A. J. Austin, R. Cammi, C. Pomelli, J. W. Ochterski, P. Y. Ayala, K. Morokuma, G. A. Voth, P. Salvador, J. J. Dannenberg, V. G. Zakrzewski, S. Dapprich, A. D. Daniels, M. C. Strain, O. Farkas, D. K. Malick, A. D. Rabuck, K. Raghavachari, J. B. Foresman, J. V. Ortiz, Q. Cui, A. G. Baboul, S. Clifford, J. Cioslowski, B. B. Stefanov, G. Liu, A. Liashenko, P. Piskorz, I. Komaromi, R. L. Martin, D. J. Fox, T. Keith, M. A. Al-Laham, C. Y. Peng, A. Nanayakkara, M. Challacombe, P. M. W. Gill, B. Johnson, W. Chen, M. W. Wong, C. Gonzalez, J. A. Pople, *Gaussian 03, Revision C.02*, Gaussian, Inc., Wallingford, CT (2004).

25. J. Stare, J. Mavri, *Comp. Phys. Comm.* **2002**, *143*, 222–240.
26. J. Stare, A. Jezierska, G. Ambrožič, I. J. Košir, J. Kidrič, A. Koll, J. Mavri, D. Hadži, *J. Am. Chem. Soc.* **2004**, *126*, 4437–4443.
27. W. H. Press, S. A. Teukolsky, W. T. Vetterling, B. P. Flannery, *Numerical Recipes*, Cambridge University Press, 1992.
28. D. Shepard, *Proceedings of the 1968 ACM National Conference*, **1968**, 517–524.
29. R. J. Renka, *ACM Transactions on Mathematical Software (TOMS)*, **1988**, *14*.

## Povzetek

Z zelo zanesljivim kvantno kemijskim pristopom (metoda sklopljenih skupkov, angl. Coupled Cluster) in velikim baznim setom smo izračunali polno, tridimenzionalno potencialno ploskev izoliranega hidrogendifluoridnega aniona ( $\text{FHF}^-$ ) v osnovnem elektronskem stanju [račun CCSD(T)/aug-cc-pVTZ]. Vrednosti potenciala smo ocenili v več kot 30.000 točkah, ki ustrezajo različnim geometrijam sistema. Analitično obliko potenciala smo zasnovali v internih koordinatah, in sicer razdalji F...F (koordinata  $R$ ) ter longitudinalni in transverzalni projekciji položaja protona na zveznico F...F (koordinati  $x$  in  $y$ ). Za vsako konstantno vrednost koordinate  $x$  smo napravili analitično prilagajanje vzdolž koordinat  $y$  in  $R$ , pri čemer smo uporabili linearno kombinacijo dvodimenzionalnih Gaussovih funkcij. Prilagojene parametre Gaussovih funkcij smo nato z metodo kubičnih zlepkov interpolirali vzdolž koordinate  $x$ . Največje odstopanje modelne funkcije od izračunanega potenciala znaša v območju nizke energije (do 20 kcal/mol nad minimumom) le 0.01 kcal/mol. Analitična oblika potenciala je zelo natančna in primerna za napredne računske študije kot npr. polno anharmonsko vibracijsko analizo ali kvandnodinamsko simulacijo.